Chemical conversions within the Mo-Ga-C system: Layered solids with variable Ga content

Carina Büchner[a,#], Niels Kubitza[a,#], Ali M. Malik[b], John Jamboretz[c], Aysha A. Riaz[d], Yujiang Zhu[d], Christoph Schlueter[e], Martha R. McCartney[f], David J. Smith[f], Anna Regoutz[d], Jochen Rohrer[b], and Christina S. Birkel[a,c,]*

[a] Department of Chemistry and Biochemistry, Technische Universität Darmstadt, 64287 Darmstadt, Germany

[b] Institute of Materials Science, Technische Universität Darmstadt, 64287 Darmstadt, Germany

[c] School of Molecular Sciences, Arizona State University, Tempe, 85281, AZ, USA

[d] Department of Chemistry, University College London, 20 Gordon Street, London WC1H 0AJ, United Kingdom.

[e] Deutsches Elektronen-Synchrotron DESY, 22607 Hamburg, Germany.

[f] Department of Physics, Arizona State University, Tempe, AZ 85281, USA

[#] Authors contributed equally

[*] Corresponding author, christina.birkel@asu.edu

ABSTRACT

Layered carbides are fascinating compounds due to their enormous structural and chemical diversity as well as their potential to possess useful and tunable functional properties. Their preparation, however, is challenging and forces synthesis scientists to develop creative and innovative strategies to access high-quality materials. One unique compound amongst carbides is Mo_2Ga_2C. Its structure is related to the large and steadily growing family of 211 MAX phases that crystallize in a hexagonal structure (space group $P6_3/mmc$) with alternating layers of edge-sharing M_6X octahedra and layers of the A element. Mo_2Ga_2C also crystallizes in the same space group, with the difference that the A-element layer is occupied by two A-elements, here Ga, that sit right on top of each other (hence named "221" compound). Here, we propose that the Ga-content in this compound is variable between 2:2, 2:1, and 2:≤1 (and 2:0) Mo:Ga ratios. We demonstrate that one Ga-layer can be selectively removed from Mo_2Ga_2C without jeopardizing the hexagonal $P6_3/mmc$ structure. This is realized by chemical treatment of the 221 phase Mo_2Ga_2C with a Lewis acid leading to the "conventional" 211 MAX phase Mo_2GaC. Upon further reaction with $CuCl_2$, more Ga is removed and replaced with Cu (instead of fully exfoliating into the Ga-free Mo_2CT_x MXene) leading to $Mo_2Ga_{1-x}Cu_xC$ still crystallizing with space group $P6_3/mmc$, however, with a significantly larger c lattice parameter. Furthermore, 211 Mo_2GaC can be reacted with Ga to recover the initial 221 Mo_2Ga_2C. All three reaction pathways have not been reported before and are supported by powder X-ray diffraction, electron microscopy, X-ray spectroscopy, and density functional theory calculations.

INTRODUCTION

The structural variety of carbides is large. The group of MAX phases, formerly known as "*H*" phases[1], is an interesting group of carbides and (carbo)nitrides which crystallize in a layered structure and combine metallic and ceramic properties within one substance class.[2] *M* is an (early) transition metal,[3–7] *A* an element of the groups 13-16[2,8] and *X* is carbon, nitrogen[2] or in rare cases boron[8]. MAX phases crystallize in a hexagonal structure (space group $P6_3/mmc$). Their chemical composition can be stated by the general sum formula $M_{1+n}AX_n$.[9] They consist of layers of edge-shared M_6X octahedra interleaved with monoatomic layers of the *A*-element. The number of interconnected *M*-*X*-layers is commonly stated by the parameter *n* and can be as high as 4.[10] The crystal structure as well as electronic structure of MAX phases, the possibility to vary the number of *M*-*X*-layers and the large variety in chemical composition makes them highly promising candidates for a wide variety of applications.[11]

A layered carbide with very similar structure and the sum formula Mo_2Ga_2C was discovered in 2015.[12] Instead of a single atomic *A*-element layer, the material has a double *A*-element layer between the *M*-*X*-layers. Both *A*-atoms are aligned in the *c*-direction. The octahedral *M*-*X*-layers with $n = 1$ have the same structure/constitution as the *M*-*X*-layers in conventional MAX phases (space group $P6_3/mmc$).[12,13] Thus, this compound can be considered as a double *A*-element MAX phase, but not satisfying the general MAX phase sum formula $M_{n+1}AX_n$.[2] Therefore, it is called a MAX-like phase or a "221 phase". Recently, Nb_2Bi_2C a compound with the same structure has been discovered, and theoretical calculations propose more similar compounds to be stable (e.g., V_2Ga_2C).[14,15] Similar compounds with two *A*-layers are $Ti_3Au_2C_2$[3] which has been synthesized in

the form of thin films, and $Ti_3Cd_2C_2$[14]. However, both materials have different structure and composition than the 221 phase.

The equivalent 211 MAX phase would be Mo_2GaC. The two structures are compared in **Figure 1**.[16] While the synthesis of "221" Mo_2Ga_2C from Mo_2C and gallium is relatively straightforward when reaction temperatures are chosen correctly,[17] the synthesis of MAX phase Mo_2GaC seems to be more challenging. The bulk 211 phase Mo_2GaC is only mentioned in a few publications. These include two reports dating from the 1960s[16,18] and a paper focusing on Raman spectroscopy with an impure sample[19]. In a doctoral thesis[20] and a further publication about synthesis parameters,[21] Mo_2GaC was synthesized from the elements as well as from Mo_2C and gallium exhibiting only minor impurities.

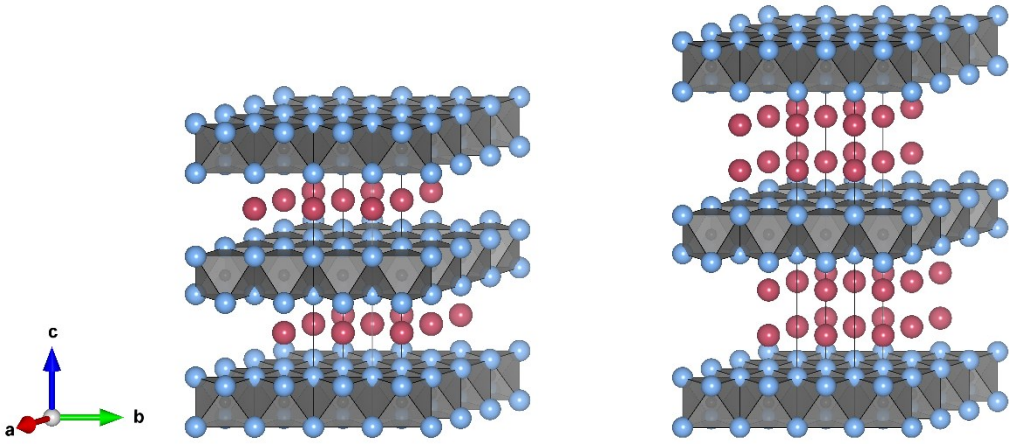

Figure 1. Crystal structure of Mo_2GaC[18] (left) and Mo_2Ga_2C[12] (right), blue: molybdenum, purple: gallium, black (center of octahedrons): carbon. The models of the crystal structures have been prepared using the software VESTA.[22]

The fact that the *M*-*X*-layers of MAX phases are only weakly bound to the *A*-layers makes a modification of the *A*-layers under conservation of the *M*-*X*-layer structure possible. An approach that can either remove the *A*-layers completely which converts the MAX phase to a MXene or

replace the *A*-element by a respective transition metal is the so-called Lewis acid transition metal salt approach.[5,23–26] During thermal treatment, the transition metal from the Lewis acid salt oxidizes the *A*-element of the MAX phase. The *A*-element gets dissolved in the mixture of the Lewis acid salt and a eutectic mixture of alkaline metal chlorides leading to the two-dimensional MXene. The transition metal of the reacting salt, is reduced to its metallic form.[26] Different oxidizers can be used to remove the latter from the product phase. For example, to oxidize copper, ammonium persulfate can be used as an oxidant. In the literature the copper residuals are described as copper clusters of a few atoms on the MXene surface.[26] The Lewis acid molten salt exfoliation method has been used for a row of aluminum and zinc[23] containing MAX phases as well as for Ti_3SiC_2 and Ti_2GaC whereas not much data is provided for the Ti_2GaC etching approach.[26] However, no experiments in which Mo_2Ga_2C or Mo_2GaC were treated with transition metal salts have been reported.

In this paper we demonstrate the selective removal of one Ga layer from Mo_2Ga_2C to access the 211 MAX phase Mo_2GaC whose solid-state synthesis has proven to be challenging. While etching with hydrofluoric acid leads to a complete removal of gallium[27] from the Mo_2Ga_2C structure forming the 2D MXene Mo_2CT_x, we use a Lewis acid ($CuCl_2$ or AgCl) to obtain Mo_2GaC from Mo_2Ga_2C. Interestingly, Mo_2Ga_2C can be recovered by the reaction of Mo_2GaC and metallic gallium. Furthermore, by treating Mo_2GaC with an excess of $CuCl_2$ a further decrease of the gallium content up to 50 % in Mo_2GaC is possible. Our data suggest that Cu is incorporated as a new *A*-element and we refer to this compound as $Mo_2Ga_{1-x}Cu_xC$. The products are structurally characterized by powder X-ray diffraction experiments and electron microscopy, the chemical environments are verified by X-ray spectroscopy techniques, and the formation of the different compounds is theoretically verified by DFT calculations.

EXPERIMENTAL SECTION

Materials preparation

During the following syntheses, no uncommon hazards are noted.

Synthesis of Mo_2Ga_2C (including reaction of Mo_2GaC and Ga)

The exact ratios, masses and synthesis conditions for all experiments are listed in the SI in **Tables S1**-**S5**.[28] All preparation steps until otherwise stated were conducted under argon. Prior to the synthesis of the 221 phase, the precursor Mo_2C was first synthesized from the elements (Mo, -325 mesh, Thermo Fisher Scientific Chem. Inc., 99.997 %; C, -325 mesh, Alfa Aesar, UCP-2 grade, ultra "F" purity). The transition metal and graphitic carbon were mixed in a ratio of 2:1 and ground using an agate mortar and pestle. The powders were pressed into a cylindrical pellet (Ø = 15 mm, 5 t, 40 sec)) and sealed in a fused silica ampule under vacuum. The ampule was placed vertically into 7 g granulated carbon (Activated charcoal, DARCO, 12-20 mesh, Sigma Aldrich) as a susceptor surrounded by an alumina crucible and an alumina fiber sheath inside a laboratory microwave oven (Mars 6 – CEM). The pellet was reacted at 1200 W for 45 min which corresponds to 1160-1390 °C. After cooling to room temperature, the dark grey pellet was ground in air until a fine powder was obtained, and its phase purity confirmed by X-ray diffraction (**Figure S1**).

Mo_2Ga_2C was synthesized according to He *et al*.[17] For the synthesis of the 221 phase, granulated gallium (Thermo Fisher Scientific Chem. Inc., 99.99 %) was sandwiched between the respective Mo_2C or Mo_2GaC powder with a large excess of gallium (at least 1:5) in a steel die (for exact amounts refer to **Table S2**). In order to distribute the gallium homogeneously, no individual gallium layer was higher than 4mm, otherwise multilayers between the carbide and gallium were

prepared and slightly pressed using a pellet die until a uniform pellet is produced. The pellet was placed inside a fused silica ampule and sealed under vacuum. The reaction mixture was thermally treated in a box furnace (CWF 12/5–Carbolite-Gero) at 685 °C for 60 h for the formation of Mo_2Ga_2C from Mo_2C and Ga, and 75 h for the reaction starting from Mo_2GaC and Ga (heating rate: 10 °C/min, cooling: natural). The actual temperature of the furnace that was measured by an external thermocouple was 665-672 °C. After the synthesis excess gallium was dissolved with concentrated hydrochloric acid for several hours. The sample was washed with water, dried in air, and ground using an agate mortar and pestle. Raman studies (**Figure S19**) and powder X-ray diffraction data (**Figure S2** and **S9**, **Table S6** and **S11**) confirm the product formation. Additionally, thermal decomposition experiments were conducted to investigate the thermal behavior of the Mo_2Ga_2C phase (SI).

Synthesis of Mo_2GaC

The respective powder of the 221 phase was ground in air with $CuCl_2*2H_2O$ (or AgCl) ($CuCl_2*2H_2O$, Ward's Science, lab grade; AgCl, Thermo Fisher Scientific Chem. Inc., 95 %) and the alkaline salts (KCl and LiCl) (KCl, Fisher Scientific, 99.9 %; LiCl, Alfa Aesar, 99 %) using an agate mortar and pestle. The exact masses, reactants and ratios are listed in **Table S3**. Due to the high hygroscopicity the powders were not ground for more than 3 min and immediately placed into an alumina boat that was placed into the furnace under argon. A horizontal tube furnace (EZS-3G 12/600B–Carbolite-Gero) was used with an argon flow rate of 0.35 L/min (flowmeter calibrated for water). The reaction times and temperatures can be found in **Table S3** and the heating rate was 5 °C/min. Optimized conditions for the reaction of Mo_2Ga_2C with $CuCl_2$ were found to be at 400 °C for 6-7 h. After cooling to room temperature, the reaction product was found slightly sintered, dark grey in color with a coppery shine. In order to remove all side products and

side phases, multiple washing steps were added: The product was soaked in water for 30 min and subsequently washed with water using a centrifuge 2-3 times (50 mL per wash, 3500 rpm, 5 min). Afterwards, the sample was immersed in hydrochloric acid (HC, concentrated, ACS grade, 36.5-38%, VWR BDH chemicals) over two days. The acid turned yellow during that time. The HCl was removed by washing the sample with water using centrifuge. To remove possible MoO_2 impurities, the sample was washed in highly diluted aqueous nitric acid (HNO_3, concentrated, certified ACS plus, Fisher Chemical) solution. Since the sample also dissolves in HNO_3 it was important to adjust the HNO_3 concentration in a way that bubbles only form slightly and that the sample only sits in the acid for a couple of minutes. This method resulted in a slight loss of the MAX phase product. To remove the HNO_3 solution, the samples were washed with water using the centrifuge. The centrifuge tubes were first filled with ~50 mL of DI water, before they were rotated in the centrifuge for 3 min with a speed of 3500 rpm. The liquid was dumped. This procedure was repeated 3-4 times.

Materials characterization

For X-ray powder diffraction analysis (Bruker D2 Phaser, 2ndGeneration) a Bragg-Brentano geometry was used with Cu $K_{\alpha,1}$-radiation (λ = 1.5406 Å), and a LYNXEYE 1D SDD detector in a range of 2θ = 5–90 ° in 0.035 °increments. 4-7 ranges were measured and added. For Rietveld refinements of the X-ray diffraction data (at least 6 ranges) the software Topas 6[29] (Bruker AXS) was used. The refinements were based on the structure models from the respective literature of Mo_2Ga_2C[12] and Mo_2GaC[18]. The lattice parameters were refined using LaB_6 powder (NIST, 660c) as a standard. Afterwards, the extracted lattice parameters were used in a Le Bail refinement

procedure based on the above stated structure models providing the suggested space group $P6_3/mmc$. The sample profile was refined using the modified Thompson-Cox-Hastings pseudo-Voigt function ((pV-TCHZ), refinement of u, v, w, and x) approach.

For scanning electron microscopy (SEM), the sample was attached to carbon tape and measured using a Zeiss Auriga FIB SEM with an Oxford Instruments SDD detector (Ultim MAX). The acceleration voltage was 5 keV for SEM images and 20 keV for energy-dispersive X-ray spectroscopy (EDS). A map as well as 10-16 point measurements were conducted for the EDS measurements. The values were normalized based on two molybdenum atoms per sum formula. Carbon was not quantified due to its low atomic number, the sample preparation on carbon tape and possible carbon contamination inside the instrument. From the point measurements, a standard deviation was calculated which refers to the sum formula.

Samples suitable for electron microscopy observation were prepared by crushing powder with a mortar and pestle under isopropanol, and then placing a drop of the suspension onto a holey carbon support film. Observations were made using an image-corrected Thermo Fisher 80-300 TEM operated at 300kV.

Non-spin polarized density functional theory (DFT) calculations were performed employing the projector augmented wave (PAW)[30] using the open source DFT code gpaw.[31,32] Electronic exchange and correlation (XC) was treated by generalized gradient approximation (GGA) in the parametrization of Perdew, Burke and Ernzerhof (PBE).[33] The energy cut-off for the plane wave expansion of the wave functions was set to the converged value of 500 eV. The Brillouin zone was sampled by Monkhorst-Pack type k-meshes with a density of 7 Å. Both cell and atom positions were optimized until stresses and forces converged within 0.01 eV $Å^{-1}$ and 0.01 eV $Å^{-3}$,

respectively. For electronic self-consistency cycle, the default settings were used for convergence. Symmetrically unique structures of $Mo_2Ga_{1-x}Cu_xC$ in super cell sizes (2,2,1) and (3,3,1) are generated using ICET[34]. A few of these configurations at each x are randomly selected and submitted to the DFT code under periodic boundary conditions. It should be noted that the random selection procedure will most likely not result in the ground state configuration. To investigate the ground state, cluster expansion[34] is required, which is beyond the scope of the present study.

Hard X-ray photoelectron spectroscopy (HAXPES) was used to characterize the chemical environments and oxidation states within the sample bulk. The HAXPES data were collected at beamline P22 at PETRAIII, German Electron Synchrotron DESY in Hamburg, Germany.[35] A photon energy of 6 keV was used for all experiments, with the energy selected using a Si (111) double-crystal monochromator. A Phoibos 225HV analyzer (SPECS, Berlin, Germany) was used with the small area lens mode and a slit size of 3 mm. Spectra were collected using a pass energy of 30 eV. The total energy resolution in this setup was determined to be 245 meV 16/84% Fermi edge (E_F) width of a polycrystalline gold foil.

In addition to HAXPES data, complementary soft X-ray photoelectron spectroscopy (SXPS) was conducted to provide a surface perspective and to explore the Cu and Cl states. SXPS data were recorded on a Thermo Scientific K-Alpha X-ray Photoelectron Spectrometer (XPS) system using a monochromated, microfocused Al Kα X-ray source (hv= 1.4867 keV, further referred to as 1.5 keV for simplicity) and a 180° double-focusing hemispherical analyzer with a 2D detector. The X-ray source was operated at 6 mA emission current and 12 kV anode bias. Data was collected using a 400 μm X-ray spot and a pass energy of 20 eV.

RESULTS AND DISCUSSION

Mo_2Ga_2C was initially synthesized according to the method of He *et al* [17] exhibiting minor side phase peaks which may be attributed to trace amounts of oxide impurities occurring due to oxygen impurities during the synthesis process. For the removal of gallium, Mo_2Ga_2C is reacted with the transition metal salts, AgCl at 550 °C and $CuCl_2$ at 400 °C, respectively. Both options are discussed separately below.

Reaction of Mo_2Ga_2C with AgCl

The reaction of Mo_2Ga_2C with AgCl (5 h, 550 °C) leads to MAX phase Mo_2GaC, as can be observed in the X-ray diffraction data (**Figure S3**). The main side product is elemental silver according to the following reaction equation:

$$Mo_2Ga_2C + 3\ AgCl \rightarrow Mo_2GaC + GaCl_3 + 3\ Ag \qquad \text{(equ. 1)}$$

Thus, one gallium layer was selectively removed from the "221" structure but no full exfoliation into MXene took place. The conversion of Mo_2Ga_2C to Mo_2GaC by using a molten transition metal salt has not been reported before and opens a new and simple way to synthesize the not easily accessible Mo_2GaC. The following can be found in the literature: There is only one publication in which Mo_2GaC has been named as a side phase in the reaction products of Mo_2Ga_2C with a molten metal,[36] but the phase is hard to identify using the XRD pattern due to overlap with other reflections. Moreover, the paper focused on the stability in general and wettability of Mo_2Ga_2C in molten metals and less on the fundamental nature of the chemical reaction.[36]

Another similar experiment reported in literature involved the selective removal of one *A*-element layer in the thin film by reaction with a thin metal layer that goes along with an *A*-element replacement reaction, namely the reaction of $Ti_3Au_2C_2$ with Ir to Ti_3IrC_2.[3] However, the selective removal of one *A*-element layer has been reported for MAB phases, mainly for the reaction of MoAlB to Mo_2AlB_2 by Brønsted acids or bases.[37–39] Due to the high redox potential of the silver byproduct, it is challenging to remove this side phase from the reaction product. Thus, $CuCl_2$ was used as an alternative Lewis acid.

Reaction of Mo_2Ga_2C with $CuCl_2$

The reaction of Mo_2Ga_2C with $CuCl_2$, when performed under the same reaction conditions as the reaction with AgCl (5 h, 550 °C), leads to Mo_2C as the main product (**Figure S4**). After optimization of the reaction conditions, successful etching was achieved at lower temperature (400 °C) according to the following reaction equation [26]:

$$Mo_2Ga_2C + 3/2\ CuCl_2 \rightarrow Mo_2GaC + GaCl_3 + 3/2\ Cu \qquad \text{(equ. 2)}$$

The X-ray powder diffraction data (**Figure 2**) show the conversion of Mo_2Ga_2C (dark blue line in **Figure 2**) to MAX phase Mo_2GaC (maroon line in **Figure 2**) upon reaction with $CuCl_2$ which in turn converts into elemental Cu (indicated by the stars in **Figure 2**) and $GaCl_3$. Elemental copper is then removed by washing with HCl which leads to essentially single-phase MAX phase Mo_2GaC (orange line in **Figure 2**) that only contains trace amounts of unreacted precursor Mo_2Ga_2C.

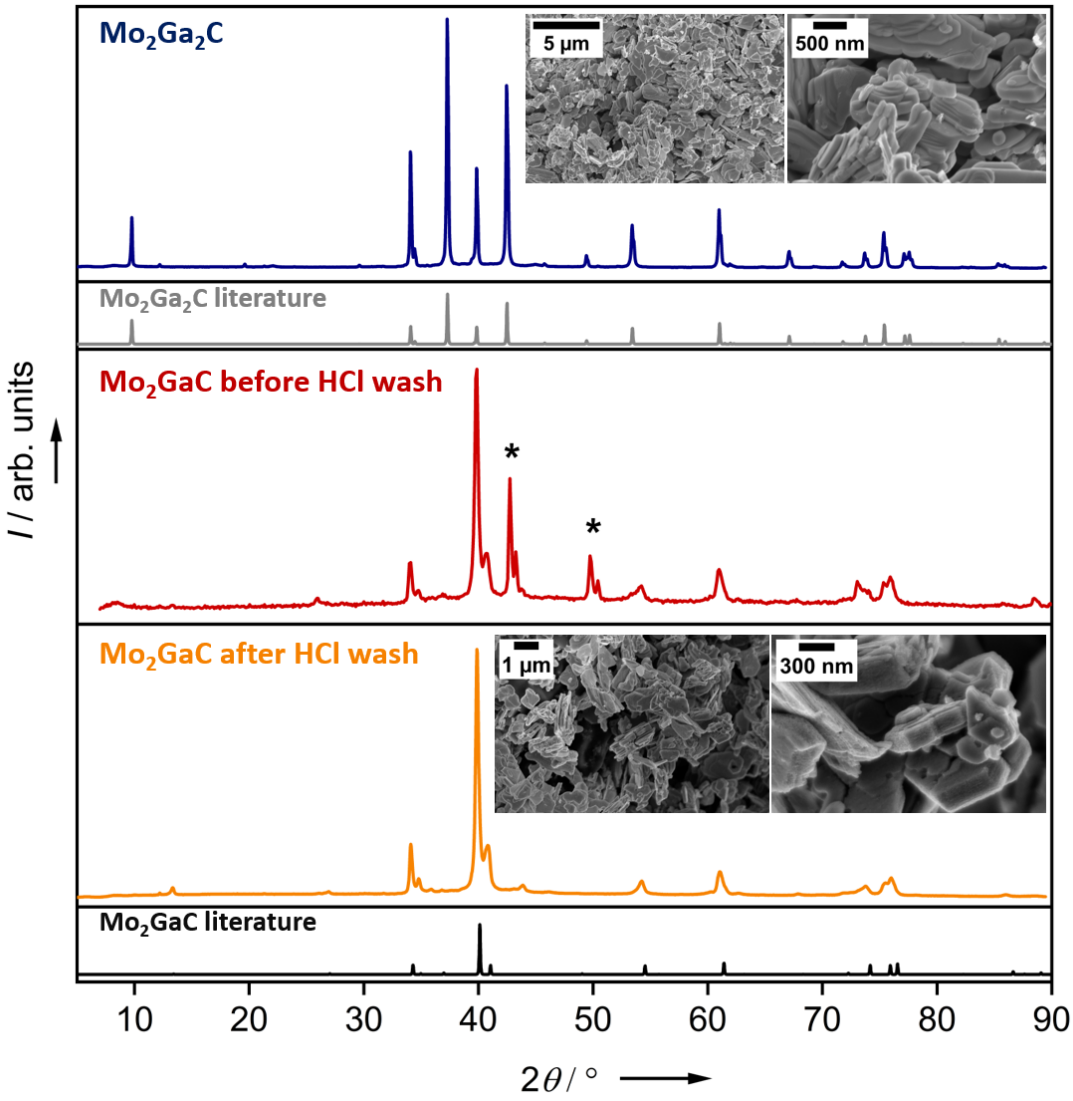

Figure 2. Transformation of the 221 phase (top) into the 211 phase (center) with subsequent washing to remove elemental Cu (bottom). From bottom to top: Experimental XRD data of 221 Mo_2Ga_2C (dark blue) with simulated XRD data of Mo_2Ga_2C (grey),[12] including SEM images of Mo_2Ga_2C (Further images can be found in the SI); experimental XRD data of as-prepared 211 Mo_2GaC (maroon, stars indicate reflections of Cu[40]) with simulated XRD data of Mo_2GaC (black)[18]; experimental XRD data of Mo_2GaC (orange) after removal of Cu including SEM images of the final Mo_2GaC product.

Le Bail refinement of the XRD data (**Figure S5**) verify the consistency of the structure with the previously published structural data of Mo_2GaC.[18] The experimentally determined lattice parameters $a = 3.0349(2)$ Å and $c = 13.287(2)$ Å are close to the parameters published by Jeitschko *et al*. ($a = 3.017$ Å and $c = 13.180$ Å).[18] Structural parameters are listed in **Table S7**. Element-specific characterization by EDS indicates that the molybdenum to gallium ratio is ~2:1 as expected for the 211 MAX phase, while copper (50 % compared to gallium) is still detectable (**Table S12**) which could be present as an amorphous side phase. Small amounts of copper could also be incorporated into the MAX phase structure due to under occupation of the gallium site, which can't be fully ruled out by the given laboratory XRD data. However, the strong similarity of the lattice parameters compared to the literature model, as well as the 2:1 Mo/Ga ratio proven by EDS measurements, strongly supporting the synthesis of Mo_2GaC as desired.

The morphology of the MAX phase Mo_2GaC (**Figure 2** lower) is very similar to the morphology of Mo_2Ga_2C (**Figure 2** upper) with flat crystallites that are stacked on top of each other. At high magnification, the surface of Mo_2GaC appears rough which is likely the result of reaction with oxidizing $CuCl_2$.

Reaction of MAX phase Mo_2GaC with $CuCl_2$

MAX phase Mo_2GaC was further reacted with $CuCl_2$ to assess its potential exfoliation behavior with the Lewis acid. Interestingly, a product with a significantly different XRD pattern (**Figure 3**, red) forms, which is, however, not the fully exfoliated MXene. Rietveld refinements (**Figure S6**, **Table S8**) of the XRD data reveal that the *c*-parameter significantly increases from $c = 13.287(2)$ Å to $c = 13.518(3)$ Å, whereas the *a*-parameter slightly decreases from $a = 3.0349(2)$ Å to $a = 3.0269(3)$ Å. Elemental analysis (EDS, **Table S12**) shows a significantly

lower gallium content of under 50 % which was also observed for further samples which were reacted with an excess of $CuCl_2$. Additionally, EDS data (**Table S12**) indicate that samples after a second reaction with $CuCl_2$ or a reaction with an excess of $CuCl_2$ (further data can be found in the supporting information, **Figure S7** and **S8** and **Table S9-S10**) contain approximately twice as much copper than the samples after the first reaction. It is noteworthy that the additional amount of copper resembles approximately the initial amount of gallium that has been removed. Thus, we assume that the additional Cu quantities in this sample are incorporated into the MAX phase structure. This is furthermore supported by the increased *c* parameter due to the larger covalent radius of copper compared to gallium[41]. The respective product is referred to as $Mo_2Ga_{1-x}Cu_xC$.

The crystallites in the SEM images (**Figure 3**, lower) look similar to those visible after the first reaction with copper chloride (**Figure 3**, upper). They appear to be corroded and the crystallites look slightly expanded but not exfoliated, which is a result of the release of gallium between the layers and the increased *c*-lattice parameter.

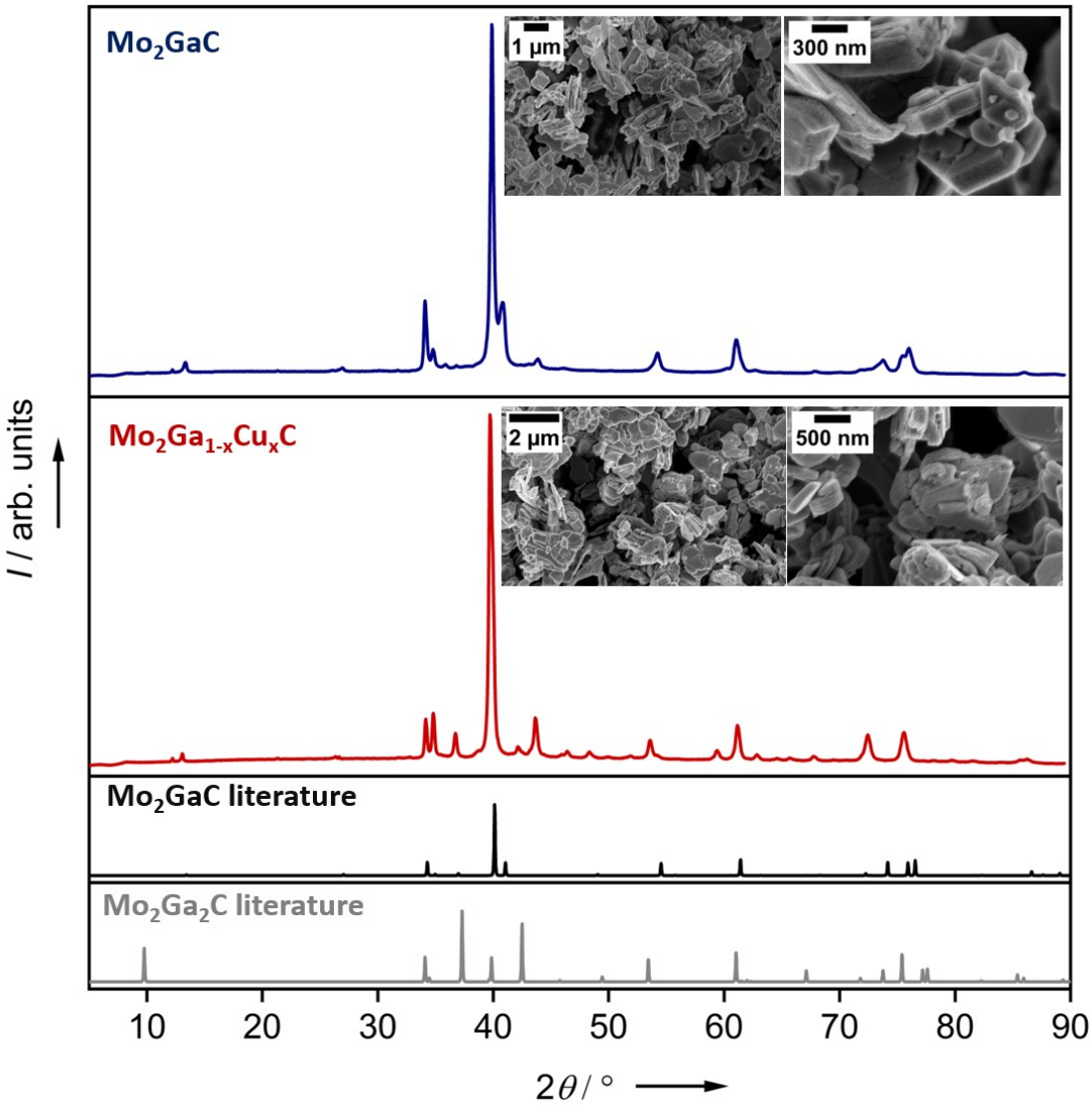

Figure 3. Conversion of 211 Mo_2GaC (top) into $Mo_2Ga_{1-x}Cu_xC$ (bottom) upon further reaction of Mo_2GaC with $CuCl_2$: Experimental XRD data of Mo_2GaC (dark blue) including SEM images, experimental XRD data of $Mo_2Ga_{1-x}Cu_xC$ (maroon) including SEM images. Simulated XRD data of Mo_2Ga_2C (grey)[12] and Mo_2GaC (black).[18]

Recovery of Mo_2Ga_2C from Mo_2GaC and gallium

MAX phase Mo_2GaC can be converted back into the starting material, the Mo_2Ga_2C "221" phase **(Figure S9** and **Table S11)**, by reaction with elemental gallium, as shown in **Figure 4**. The XRD data (**Figure 4**) and Le Bail refinements confirm a successful reincorporation of the second gallium layer and the reconstruction of phase-pure Mo_2Ga_2C. The EDS data (**Table S12**) almost nearly confirm the targeted 1:1 ratio (Mo/Ga = 1/1.145). The slight gallium excess can be explained by the significant excess of gallium used during the preparation process. Surprisingly, almost no copper can be detected in the EDS spectrum. Gallium may have reacted with copper or the copper-containing side phases and the reaction product could have been dissolved in HCl. The SEM images of the 221 product obtained from the 211 phase and gallium (**Figure 4**) look similar to the images of the 221 phase which was synthesized from Mo_2C and gallium (**Figure 4**) with flat stacked crystallites and smooth surfaces.

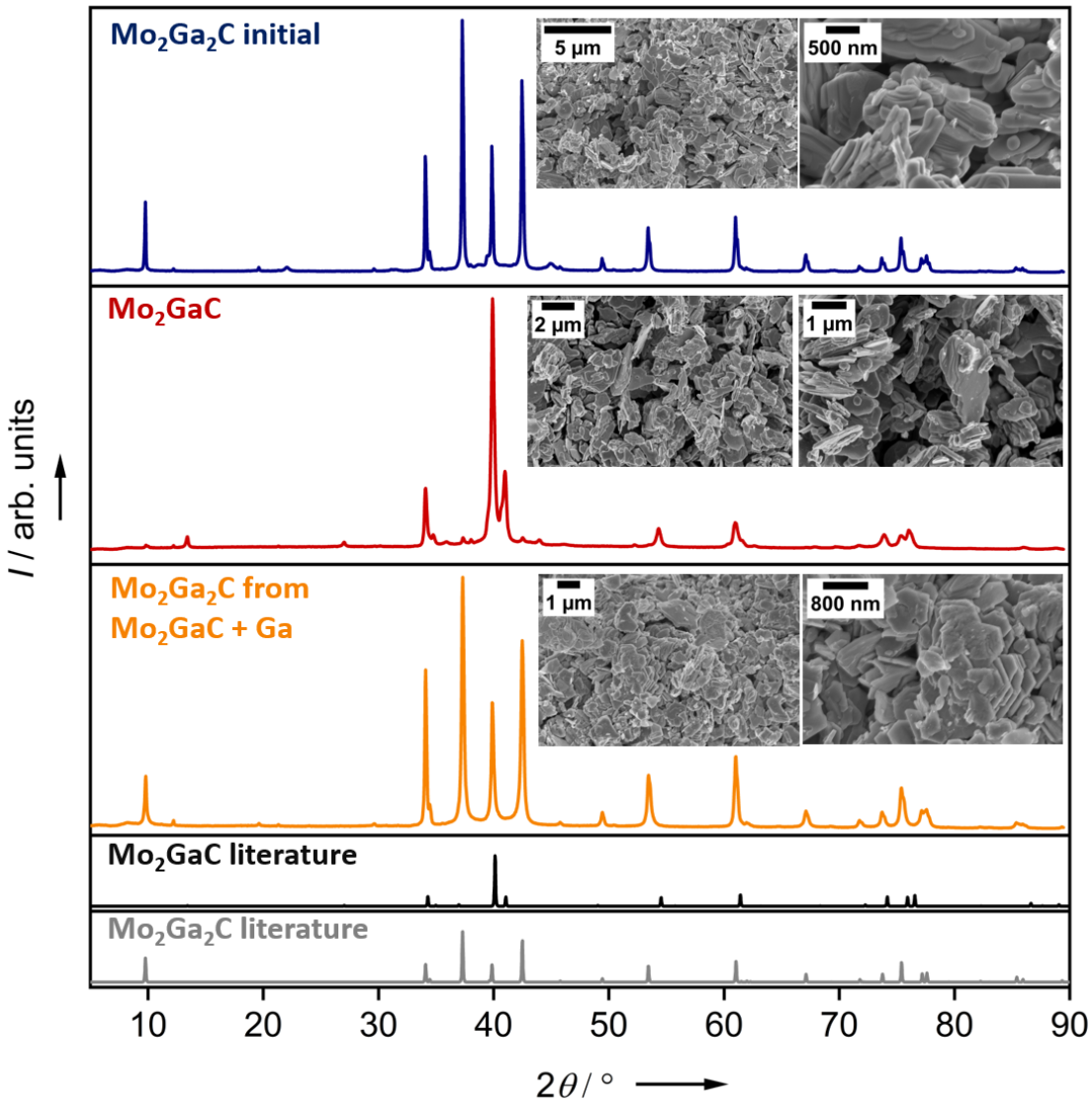

Figure 4. Transformation of 221 Mo_2Ga_2C (top) into 211 Mo_2GaC (center) and back into 221 Mo_2Ga_2C (bottom): Experimental XRD data of Mo_2Ga_2C (dark blue), Mo_2GaC (maroon), and "recovered" Mo_2Ga_2C (orange) including SEM images grey: simulated XRD data of Mo_2Ga_2C[12] black: simulated XRD data of Mo_2GaC.[18]

Transmission Electron Microscopy

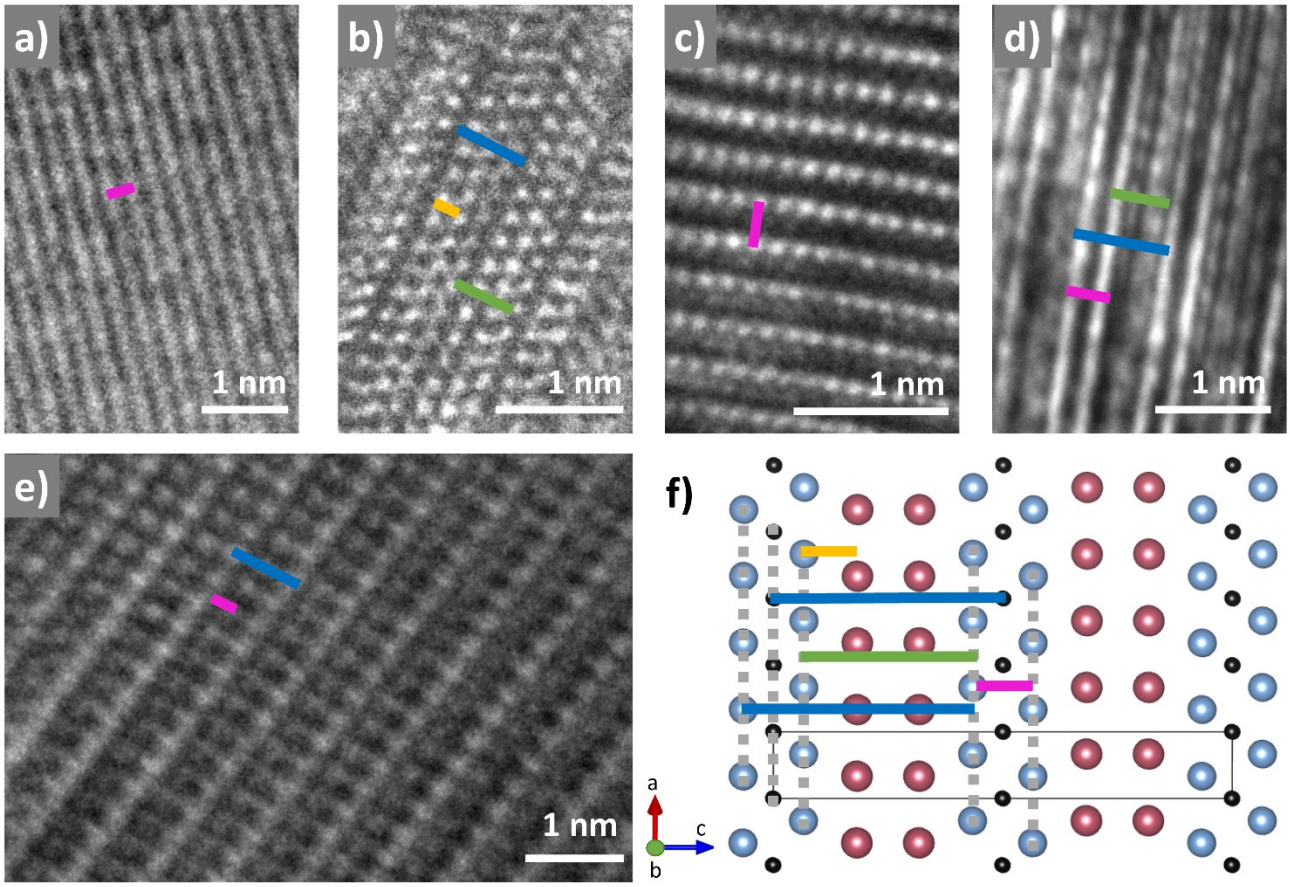

Figure 5. Transmission electron micrographs of $Mo_2Ga_{1-x}Cu_xC$ (a-c), Mo_2GaC (d and e), and schematic of the structure model of Mo_2GaC by Jeitschko *et al.*[18] with projection onto the 010 plane (f). blue: molybdenum, purple: gallium, black: carbon.

Table 1. Distances of different layer elements in the transmission electron micrographs of Mo_2GaC and $Mo_2Ga_{1-x}Cu_xC$ in comparison to the theoretical values based on the structural model of Jeitschko *et al.* [18] The subfigure labels refer to those used in Figure 5. The standard deviation σ was determined from 10-40 distance measurements.

sample	subfigure	color of marker	Theor. distance / nm[18]	distance / nm	σ / nm
$Mo_2Ga_{1-x}Cu_xC$	Mo-C-Mo	pink	0.23	0.272	0.023
$Mo_2Ga_{1-x}Cu_xC$	half unit cell	blue	0.66	0.697	0.031
$Mo_2Ga_{1-x}Cu_xC$	Mo-Ga	yellow	0.22	0.228	0.021
$Mo_2Ga_{1-x}Cu_xC$	Mo-Ga-Mo	green	0.43	0.474	0.029
$Mo_2Ga_{1-x}Cu_xC$	Mo-C-Mo	pink	0.23	0.278	0.013
Mo_2GaC	Mo-C-Mo	pink	0.23	0.244	0.019
Mo_2GaC	half unit cell	blue	0.66	0.726	0.029
Mo_2GaC	Mo-Ga-Mo	green	0.43	0.479	0.019
Mo_2GaC	Mo-C-Mo	pink	0.23	0.312	0.017
Mo_2GaC	Half unit cell	blue	0.66	0.659	0.029

Mo_2GaC and $Mo_2Ga_{1-x}Cu_xC$ were investigated by TEM to confirm their layered structure (**Figure 5**). In general, the TEM images show that the samples consist of small crystallites, often with an extended lamellar shape, as well as regions that appeared to be amorphous, which is in agreement with the relatively low reaction temperatures and the small crystal sizes that were determined by the Rietveld refinement of the XRD data (**Table S7** and **S8-9**). In crystalline areas, the layered structure of the MAX phases was clearly visible. The distances between the layered structure elements were measured perpendicular to the plane of the layers (**Table 1**) and compared to the distances of the structural elements in the structural model.[18] Considering the different unit-cell orientations, as well as slight inaccuracies in the distance determination, the measured distances between neighboring layer elements that are both either bright or dark from the micrographs, fit reasonably well with the Mo-Ga distances inside the octahedra or the distances between Mo and Ga in the model of Mo_2GaC.[18] The herringbone-like pattern which should be visible with projection onto the 100 or 010 plane can be observed in **Figure 5 b**. The Mo-Ga-Mo atom columns

can be clearly observed and the distances of the presumed Mo-Ga-Mo atoms (**Figure 5 b**, green line) fit well with the values for the model structure[18] (**Figure 5 f**, green line). The distance between two bright atomic columns that are located next to each other (**Figure 5 b**, orange line) fit well with the Mo-Ga distances (**Figure 5 f**, orange line). The distances between two spaces that separate the structural herringbone-like elements made of three bright atomic column layers adjacent to each other (**Figure 5 b**, blue line) equals half of the unit cell length (**Figure 5 f**, blue line). The same observations can be made for **Figure 5 d**. No atomic columns, only layers, are visible in this image, but the distances also fit closely to the model (**Figure 5 f**).

X-ray Spectroscopy

HAXPES was used to explore the chemical environments and oxidation states of the metals in the initial Mo_2Ga_2C (start), Mo_2GaC, and Mo_2Ga_2C prepared by the reaction of Mo_2GaC and gallium (end). Survey spectra show all expected core levels as well as the Mo_2GaC sample showing discernible signals from Cu (see **Figure S15**). Key high-resolution core state spectra were collected and are shown in **Figure 6**. The Mo 3*d* spectra (**Figure 6(a)**) are dominated by metallic Mo^0 states as expected, for the carbide phases of the three samples with the Mo $3d_{5/2}$ line at 228.0 eV. The metallic character of the formed samples is further confirmed by HAXPES valence band spectra (see **Figure S16**), which show a distinct Fermi cut-off of the filled states. In addition, smaller contributions from Mo^{+2} and Mo^{+4} oxides are present at higher binding energies (BEs) of 229.2 and 232.7 eV for the $3d_{5/2}$ lines, respectively. Complementary SXPS measurements (see **Figure S17**) confirm that these oxides are located at the surfaces of the samples by exploiting the difference in probing depth between HAXPES and SXPS. The maximum inelastic mean free path (IMFP) for model Ga_2O_3 (representative of the surface oxide in these samples) is 7.7 nm for HAXPES and only 2.5 nm for SXPS (values calculated using the Tanuma, Powell, and Penn (TPP-

2M) approach as implemented in the QUASES software package) tripling the probing depth in HAXPES compared to SXPS. The Ga $2p_{3/2}$ core line (**Figure 6(b)**) is also dominated by metallic Ga^0 states at 1116.4 eV for all samples with varying contributions from Ga oxide environments at a higher BE of 1118.2 eV. SXPS again confirms that these are surface states. A clear difference in Ga concentration relative to Mo is found with the Mo_2GaC sample showing considerably lower Ga intensity. When comparing the Ga and Mo metallic carbide contributions relative to the initial Mo_2Ga_2C sample, the resulting Mo_2GaC sample has a Mo:Ga ratio of 1:0.6, and Mo_2Ga_2C prepared by the reaction of Mo_2GaC and Ga returns to a 1:1 ratio. The C 1*s* core level spectra (**Figure 6(c)**) all show the typical low BE feature of Mo-C carbide environments at 283.8 eV as well as a varying amount of C-H states. Finally, the O 1*s* spectra (**Figure 6(d)**) confirm the presence of Ga oxide with the main oxide contribution increasing in line with the increase seen in the Ga $2p_{3/2}$ spectra. The results from photoelectron spectroscopy confirm the successful formation of Mo_2Ga_2C and Mo_2GaC as well as the return to Mo_2Ga_2C. In addition, Cu is clearly detectable in the Mo_2GaC sample. The Cu $2p_{3/2}$ core level and Cu $L_3M_{4,5}M_{4,5}$ Auger lines were collected using SXPS. The Cu $2p_{3/2}$ core level shows a BE commensurate with $Cu^{0/1+}$ states (see **Figure S18(a)**). The Cu Auger spectra only show a clear feature for sample Mo_2GaC, with a main line kinetic energy of 918.4 eV commensurate with Cu^0 and excluding Cu_2O and CuO. Whilst minute Cu signals are also found in the Mo_2Ga_2C prepared by the reaction of Mo_2GaC and Ga, they do not allow for a clear identification of oxidation state and/or chemical environment. Finally, only minute trace amounts of Cl are present in the samples (see **Figure S18(c)**).

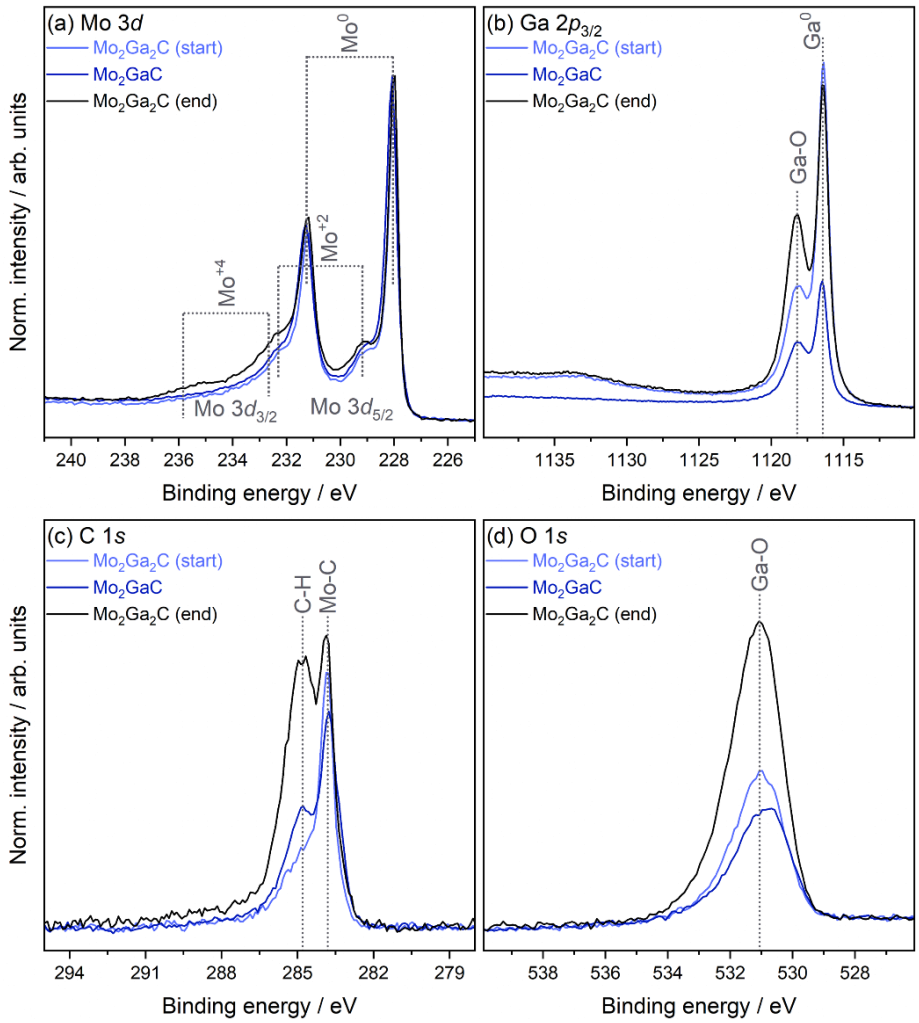

Figure 6. HAXPES core level spectra of the initial Mo_2Ga_2C (start), of Mo_2GaC, and of the Mo_2Ga_2C prepared by the reaction of Mo_2GaC and gallium (end), including (a) Mo 3*d*, (b) Ga $2p_{3/2}$, (c) C 1*s*, and (d) O 1*s*. All spectra are normalized to the main metallic feature in the Mo $3d_{5/2}$ line and aligned to the Fermi cut-off of the individual samples.

Thermodynamic stability

To theoretically confirm the formation of Mo_2GaC and the recovery of Mo_2Ga_2C, the reaction enthalpies (ΔH) were determined as,

$$\Delta H_{Mo_2GaC} = \frac{\epsilon_{Mo_2GaC} + \epsilon_{GaCl_3} + 3/2\epsilon_{Cu} - \epsilon_{Mo_2Ga_2C} - 3/2\epsilon_{CuCl_2}}{4} = -0.484 \text{ eV/atom}, \qquad \text{(equ.3)}$$

$$\Delta H_{Mo_2Ga_2C} = \frac{\epsilon_{Mo2Ga2C} - \epsilon_{Mo2GaC} - \epsilon_{Ga}}{5} = -0.051 \text{ eV/atom, respectively.} \qquad \text{(equ.4)}$$

Here, ϵ is the total DFT energy per chemical formula unit of a phase. The ΔH of both the formation of Mo_2GaC (first etching step) and the back recovery of Mo_2Ga_2C using excess Ga, have negative values (< 0) and thus both are thermodynamically favored. This finding aligns with the experimental results.

To confirm the incorporation of Cu at the Ga-sites upon excessive etching of Mo_2GaC with $CuCl_2$, the reaction enthalpy (ΔH) of the formation of a $Mo_2Ga_xCu_{1-x}C$ phase was evaluated as follows,

$$Mo_2GaC + 3x/2\ CuCl_2 \rightarrow Mo_2Ga_{1-x}Cu_xC + x\ GaCl_3 + x/2\ Cu,$$

$$\Delta H = \frac{(\epsilon_{Mo_2Ga_{1-x}Cu_xC} + x\,\epsilon_{GaCl_3} + x/2\epsilon_{Cu} - \epsilon_{Mo_2GaC} - 3x/2\,\epsilon_{CuCl_2})}{N_{atoms}}. \qquad \text{(equ.5)}$$

Here, N_{atoms} denotes the total number of atoms per chemical formula of a $Mo_2Ga_{1-x}Cu_xC$ phase.

Figure 7 shows the calculated reaction enthalpies of the formation reactions of Cu-containing $Mo_2Ga_{1-x}Cu_xC$ phases with varying concentrations of Cu (x in **Figure 7**). ΔH exhibits a negative (< 0) value for each phase and decreases with increasing Cu concentration attaining a minimum at x=1.0 (right bottom in **Figure 7**). This indicates that Cu incorporation is thermodynamically feasible and Cu-containing $Mo_2Ga_{1-x}Cu_xC$ phases are (meta)stable. These findings verify the presence of Cu inside the Mo_2GaC phase upon enhanced etching and align with the experimental

observation. Further considerations regarding the respective theoretical lattice parameters and phonon band structure and electron density of states can be found in the Supporting Information (**Figure S23-S27**).

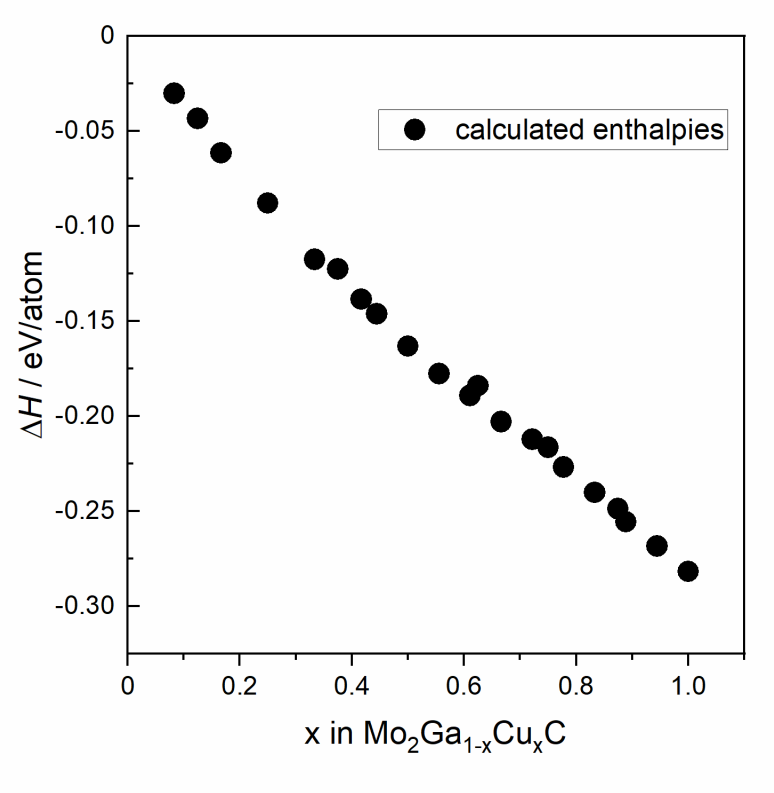

Figure 7. Calculated reaction enthalpies (ΔH) of formation of Cu-containing $Mo_2Ga_{1-x}Cu_xC$ phases with varying concentrations of Cu (x) inside the structure. The enthalpy change of all Cu-containing phases is negative, suggesting the presence of Cu atoms inside the structure. It should be noted that the mixed Cu-containing phases may not depict the true convex hull due to random sampling but can be considered as an upper limit of the convex hull line.

CONCLUSIONS

We present three hitherto unknown chemical conversion approaches within the Mo-Ga-C system that are centered around a variable Ga content: (i) "221" Mo_2Ga_2C – that is the state-of-the-art precursor for Mo_2CT_x MXene and structurally almost one of its kind – is reacted with a Lewis acid, e.g., $CuCl_2$, to form the 211 MAX phase Mo_2GaC. This is an elegant way to synthesize the latter which has been challenging to obtain by solid-state reactions. (ii) Interestingly, Mo_2GaC can be reacted with Ga to recover the initial "221" compound. (iii) The variability of Ga in this particular system is further demonstrated by reacting MAX phase Mo_2GaC with additional $CuCl_2$ leading to further removal of Ga with simultaneous incorporation of Cu on the *A*-site in the layered structure. The product $Mo_2Ga_{1-x}Cu_xC$ exhibits a significantly larger *c*-lattice parameter than Mo_2GaC while the hexagonal structure with space group $P6_3/mmc$ is maintained. The stability of all (new) compounds is confirmed by DFT calculations, and the products are structurally characterized by diffraction and microscopy techniques and their elemental constituents and chemical states are confirmed by X-ray photoelectron spectroscopy. The new reaction pathways reported here may lead to the discovery of further "221" and Ga-deficient compounds and may be transferable to other carbides that form layered structures, even beyond the family of MAX and MAX-related phases.

AUTHOR INFORMATION

Corresponding Author

*christina.birkel@asu.edu

Author Contributions

The manuscript was written through contributions of all authors. All authors have given approval to the final version of the manuscript.

Funding Sources

This work has been supported by the Deutsche Forschungsgemeinschaft (DFG, German Research Foundation) within CRC/TRR 270 (Project-ID 405553726) and by a DFG proposal with Project-ID 501386284.

A.A.R acknowledges the support from the Department of Chemistry, UCL. A.R. acknowledges support from the Analytical Chemistry Trust Fund for her CAMS-UK Fellowship.

AR acknowledges the support from the Institute of Physics (IOP) carer's fund, which provided financial support to enable her to attend the HAXPES experiments at PETRA III in person.

ACKNOWLEDGMENT

We acknowledge the use of facilities within the Eyring Materials Center at Arizona State University supported in part by NNCI-ECCS-1542160.

We acknowledge DESY (Hamburg, Germany), a member of the Helmholtz Association HGF, for the provision of experimental facilities. Parts of this research were carried out at PETRA III using beamline P22. Beamtime was allocated for proposal I-20221270.

We gratefully acknowledge the computing time provided to us on the high-performance computer Lichtenberg at the NHR Centers NHR4CES at TU Darmstadt. This is funded by the Federal Ministry of Education and Research, and the state governments participating on the basis of the resolutions of the GWK for national high performance computing at universities.

ASSOCIATED CONTENT

Supporting Information. The following files are available free of charge. PDF document including experimental details, XRD and refinement data, SEM images, XPS data, Raman and thermal decomposition study, and DFT results.

REFERENCES

(1) Jeitschko, W.; Nowotny, H.; Benesovsky, F. Die H-Phasen: Ti_2CdC, Ti_2GaC, Ti_2GaN, Ti_2InN, Zr_2InN Und Nb_2GaC. *Monatsh Chem* **1964**, *95* (1), 178–179. https://doi.org/10.1007/BF00909264.

(2) Barsoum, M. W. *The M,AXN Phases: A New Class of Solids; Thermodynamically Stable Nanolaminates*; 2000; Vol. 28.

(3) Fashandi, H.; Dahlqvist, M.; Lu, J.; Palisaitis, J.; Simak, S. I.; Abrikosov, I. A.; Rosen, J.; Hultman, L.; Andersson, M.; Lloyd Spetz, A.; Eklund, P. Synthesis of Ti_3AuC_2, $Ti_3Au_2C_2$ and Ti_3IrC_2 by Noble Metal Substitution Reaction in Ti_3SiC_2 for High-Temperature-Stable Ohmic Contacts to SiC. *Nat Mater* **2017**, *16* (8), 814–818. https://doi.org/10.1038/nmat4896.

(4) Li, Y.; Li, M.; Lu, J.; Ma, B.; Wang, Z.; Cheong, L. Z.; Luo, K.; Zha, X.; Chen, K.; Persson, P. O. Å.; Hultman, L.; Eklund, P.; Shen, C.; Wang, Q.; Xue, J.; Du, S.; Huang, Z.; Chai, Z.; Huang, Q. Single-Atom-Thick Active Layers Realized in Nanolaminated $Ti_3(Al_xCu_{1-x})C_2$ and Its Artificial Enzyme Behavior. *ACS Nano* **2019**, *13* (8), 9198–9205. https://doi.org/10.1021/acsnano.9b03530.

(5) Li, Y.; Liang, J.; Ding, H.; Lu, J.; Mu, X.; Yan, P.; Zhang, X.; Chen, K.; Li, M.; Persson, P. O. Å.; Hultman, L.; Eklund, P.; Du, S.; Yang, H.; Chai, Z.; Huang, Q. Near-Room Temperature Ferromagnetic Behavior of Single-Atom-Thick 2D Iron in Nanolaminated Ternary MAX Phases. *Appl Phys Rev* **2021**, *8* (3). https://doi.org/10.1063/5.0059078.

(6) Lai, C. C.; Fashandi, H.; Lu, J.; Palisaitis, J.; Persson, P. O. Å.; Hultman, L.; Eklund, P.; Rosen, J. Phase Formation of Nanolaminated Mo_2AuC and $Mo_2(Au_{1-x}Ga_x)_2C$ by a Substitutional Reaction within Au-Capped Mo_2GaC and Mo_2Ga_2C Thin Films. *Nanoscale* **2017**, *9* (45), 17681–17687. https://doi.org/10.1039/c7nr03663a.

(7) Lai, C. C.; Petruhins, A.; Lu, J.; Farle, M.; Hultman, L.; Eklund, P.; Rosen, J. Thermally Induced Substitutional Reaction of Fe into Mo_2GaC Thin Films. *Mater Res Lett* **2017**, *5* (8), 533–539. https://doi.org/10.1080/21663831.2017.1343207.

(8) Rackl, T.; Eisenburger, L.; Niklaus, R.; Johrendt, D. Syntheses and Physical Properties of the MAX Phase Boride Nb_2SB and the Solid Solutions $NB_2SB_xC_{1-x}$(x=0-1). *Phys Rev Mater* **2019**, *3* (5). https://doi.org/10.1103/PhysRevMaterials.3.054001.

(9) Eklund, P.; Beckers, M.; Jansson, U.; Högberg, H.; Hultman, L. The $M_{n+1}AX_n$ Phases: Materials Science and Thin-Film Processing. *Thin Solid Films*. February 1, 2010, pp 1851–1878. https://doi.org/10.1016/j.tsf.2009.07.184.

(10) Deysher, G.; Shuck, C. E.; Hantanasirisakul, K.; Frey, N. C.; Foucher, A. C.; Maleski, K.; Sarycheva, A.; Shenoy, V. B.; Stach, E. A.; Anasori, B.; Gogotsi, Y. Synthesis of Mo_4VAlC_4 MAX Phase and Two-Dimensional Mo_4VC_4 MXene with Five Atomic Layers of Transition Metals. *ACS Nano* **2020**, *14* (1), 204–217. https://doi.org/10.1021/acsnano.9b07708.

(11) Gonzalez-Julian, J. Processing of MAX Phases: From Synthesis to Applications. *Journal of the American Ceramic Society* **2021**, *104* (2), 659–690. https://doi.org/10.1111/jace.17544.

(12) Hu, C.; Lai, C. C.; Tao, Q.; Lu, J.; Halim, J.; Sun, L.; Zhang, J.; Yang, J.; Anasori, B.; Wang, J.; Sakka, Y.; Hultman, L.; Eklund, P.; Rosen, J.; Barsoum, M. W. Mo_2Ga_2C: A New Ternary Nanolaminated Carbide. *Chemical Communications* **2015**, *51* (30), 6560–6563. https://doi.org/10.1039/c5cc00980d.

(13) Lai, C. C.; Meshkian, R.; Dahlqvist, M.; Lu, J.; Näslund, L.; Rivin, O.; Caspi, E. N.; Ozeri, O.; Hultman, L.; Eklund, P.; Barsoum, M. W.; Rosen, J. Structural and Chemical Determination of the New Nanolaminated Carbide Mo_2Ga_2C from First Principles and Materials Analysis. *Acta Mater* **2015**, *99*, 157–164. https://doi.org/10.1016/j.actamat.2015.07.063.

(14) Ding, H.; Li, Y.; Li, M.; Chen, K.; Liang, K.; Chen, G.; Lu, J.; Palisaitis, J.; Persson, O. Å.; Hultman, L.; Du, S.; Chai, Z.; Gogotsi, Y.; Huang, Q. *Chemical Scissor-Mediated Structural Editing of Layered Transition Metal Carbides*; 2023; Vol. 379. https://doi.org/10.1007/s40843-023-2488-y.

(15) Thore, A.; Dahlqvist, M.; Alling, B.; Rosen, J. Phase Stability of the Nanolaminates V_2Ga_2C and $(Mo_{1-x}V_x)_2Ga_2C$ from First-Principles Calculations. *Physical Chemistry Chemical Physics* **2016**, d 0022-5088_2867_2990055-0. *Journal of Less-Common Metals* **1967**, *13*, 129–131.

(16) J.; Ouisse, T.; Barsoum, M. W. First-Order Raman Scattering in Three-Layered Mo-Based Ternaries: MoAlB, Mo_2Ga_2C and Mo_2GaC. *Journal of Raman Spectroscopy* **2017**, *48* (5), 631–638. https://doi.org/10.1002/jrs.5087.

(17) He, H.; Jin, S.; Fan, G.; Wang, L.; Hu, Q.; Zhou, A. Synthesis Mechanisms and Thermal Stability of Ternary Carbide Mo_2Ga_2C. *Ceram Int* **2018**, *44* (18), 22289–22296. https://doi.org/10.1016/j.ceramint.2018.08.353.

(18) Jeitschko, W.; Nowotny, H.; Benesovsky, F. Kohlenstoffhaltige Ternäre Verbindungen (H-Phase). *Monatsheft für Chemie* **1963**, *94*, 672–676.

(19) Chaix-Pluchery, O.; Thore, A.; Kota, S.; Halim, J.; Hu, C.; Rosen, Phase stability of the nanolaminates V_2Ga_2C and $(Mo_{1-x}V_x)_2Ga_2C$ from first-principles calculations *18* (18), 12682–12688. https://doi.org/10.1039/c6cp00802j.

(20) Vryhof, D. Synthesis and Characterization of Mo_2GaC, Mo_2GaN and Mo_2AlC MAX Phases, PhD thesis, Drexel University **2013**.

(21) Hu, C.; Li, C.; Halim, J.; Kota, S.; Tallman, D. J.; Barsoum, M. W. On the Rapid Synthesis of the Ternary Mo_2GaC. *Journal of the American Ceramic Society* **2015**, *98* (9), 2713–2715. https://doi.org/10.1111/jace.13743.

(22) Momma, K.; Izumi, F. VESTA 3 for Three-Dimensional Visualization of Crystal, Volumetric and Morphology Data. *J Appl Crystallogr* **2011**, *44* (6), 1272–1276. https://doi.org/10.1107/S0021889811038970.

(23) Li, M.; Lu, J.; Luo, K.; Li, Y.; Chang, K.; Chen, K.; Zhou, J.; Rosen, J.; Hultman, L.; Eklund, P.; Persson, P. O. Å.; Du, S.; Chai, Z.; Huang, Z.; Huang, Q. Element Replacement Approach by Reaction with Lewis Acidic Molten Salts to Synthesize Nanolaminated MAX Phases and MXenes. *J Am Chem Soc* **2019**, *141* (11), 4730–4737. https://doi.org/10.1021/jacs.9b00574.

(24) Liu, L.; Orbay, M.; Luo, S.; Duluard, S.; Shao, H.; Harmel, J.; Rozier, P.; Taberna, P. L.; Simon, P. Exfoliation and Delamination of $Ti_3C_2T_x$ MXene Prepared via Molten Salt Etching Route. *ACS Nano* **2022**, *16* (1), 111–118. https://doi.org/10.1021/acsnano.1c08498.

(25) Dong, H.; Xiao, P.; Jin, N.; Wang, B.; Liu, Y.; Lin, Z. Molten Salt Derived Nb_2CT_x MXene Anode for Li-Ion Batteries. *ChemElectroChem* **2021**, *8* (5), 957–962. https://doi.org/10.1002/celc.202100142.

(26) Li, Y.; Shao, H.; Lin, Z.; Lu, J.; Liu, L.; Duployer, B.; Persson, P. O. Å.; Eklund, P.; Hultman, L.; Li, M.; Chen, K.; Zha, X. H.; Du, S.; Rozier, P.; Chai, Z.; Raymundo-Piñero, E.; Taberna, P. L.; Simon, P.; Huang, Q. A General Lewis Acidic Etching Route for Preparing MXenes with Enhanced Electrochemical Performance in Non-Aqueous Electrolyte. *Nat Mater* **2020**, *19* (8), 894–899. https://doi.org/10.1038/s41563-020-0657-0.

(27) Björk, J.; Halim, J.; Zhou, J.; Rosen, J. Predicting Chemical Exfoliation: Fundamental Insights into the Synthesis of MXenes. *NPJ 2D Mater Appl* **2023**, *7* (1). https://doi.org/10.1038/s41699-023-00370-8.

(28) Reddy, K. M.; Rao, T. N.; Revathi, J.; Joardar, J. Structural Stability of α/β-Mo_2C during Thermochemical Processing. *J Alloys Compd* **2010**, *494* (1–2), 386–391. https://doi.org/10.1016/j.jallcom.2010.01.055.

(29) Coelho, A. A. TOPAS and TOPAS-Academic: An Optimization Program Integrating Computer Algebra and Crystallographic Objects Written in C++: An. *J Appl Crystallogr* **2018**, *51* (1), 210–218. https://doi.org/10.1107/S1600576718000183.

(30) Blöchl, P. E. Projector Augmented-Wave Method. *Phys Rev B* **1994**, *50* (24), 17953–17979.

(31) Enkovaara, J.; Rostgaard, C.; Mortensen, J. J.; Chen, J.; Dułak, M.; Ferrighi, L.; Gavnholt, J.; Glinsvad, C.; Haikola, V.; Hansen, H. A.; Kristoffersen, H. H.; Kuisma, M.; Larsen, A. H.; Lehtovaara, L.; Ljungberg, M.; Lopez-Acevedo, O.; Moses, P. G.; Ojanen, J.; Olsen, T.; Petzold, V.; Romero, N. A.; Stausholm-Møller, J.; Strange, M.; Tritsaris, G. A.; Vanin, M.; Walter, M.; Hammer, B.; Häkkinen, H.; Madsen, G. K. H.; Nieminen, R. M.; Nørskov, J. K.; Puska, M.; Rantala, T. T.; Schiøtz, J.; Thygesen, K. S.; Jacobsen, K. W. Electronic Structure Calculations with GPAW: A Real-Space Implementation of the Projector Augmented-Wave Method. *Journal of Physics Condensed Matter* **2010**, *22* (25). https://doi.org/10.1088/0953-8984/22/25/253202.

(32) Enkovaara, J.; Romero, N. A.; Shende, S.; Mortensen, J. J. GPAW - Massively Parallel Electronic Structure Calculations with Python-Based Software. *Procedia Comput Sci* **2011**, *4*, 17–25. https://doi.org/10.1016/j.procs.2011.04.003.

(33) Perdew, J. P.; Burke, K.; Ernzerhof, M. Generalized Gradient Approximation Made Simple. *Phys Rev Lett* **1996**, *77* (18), 3865–3868.

(34) Ångqvist, M.; Muñoz, W. A.; Rahm, J. M.; Fransson, E.; Durniak, C.; Rozyczko, P.; Rod, T. H.; Erhart, P. ICET – A Python Library for Constructing and Sampling Alloy Cluster Expansions. *Adv Theory Simul* **2019**, *2* (7). https://doi.org/10.1002/adts.201900015.

(35) Schlueter, C.; Gloskovskii, A.; Ederer, K.; Schostak, I.; Piec, S.; Sarkar, I.; Matveyev, Y.; Lömker, P.; Sing, M.; Claessen, R.; Wiemann, C.; Schneider, C. M.; Medjanik, K.; Schönhense, G.; Amann, P.; Nilsson, A.; Drube, W. The New Dedicated HAXPES Beamline P22 at PETRAIII. In *AIP Conference Proceedings*; American Institute of Physics Inc., 2019; Vol. 2054. https://doi.org/10.1063/1.5084611.

(36) Du, Y.; Wang, F.; Hu, M.; Hu, Q.; Zhou, A. Stability and Wettability of Ternary Carbide Mo_2Ga_2C in Molten Metals. *Ceram Int* **2023**, *49* (13), 21449–21454. https://doi.org/10.1016/j.ceramint.2023.03.275.

(37) Alameda, L. T.; Holder, C. F.; Fenton, J. L.; Schaak, R. E. Partial Etching of Al from MoAlB Single Crystals to Expose Catalytically Active Basal Planes for the Hydrogen Evolution Reaction. *Chemistry of Materials* **2017**, *29* (21), 8953–8957. https://doi.org/10.1021/acs.chemmater.7b02511.

(38) Alameda, L. T.; Moradifar, P.; Metzger, Z. P.; Alem, N.; Schaak, R. E. Topochemical Deintercalation of Al from MoAlB: Stepwise Etching Pathway, Layered Intergrowth

Structures, and Two-Dimensional MBene. *J Am Chem Soc* **2018**, *140* (28), 8833–8840. https://doi.org/10.1021/jacs.8b04705.

(39) Alameda, L. T.; Lord, R. W.; Barr, J. A.; Moradifar, P.; Metzger, Z. P.; Steimle, B. C.; Holder, C. F.; Alem, N.; Sinnott, S. B.; Schaak, R. E. Multi-Step Topochemical Pathway to Metastable Mo_2AlB_2 and Related Two-Dimensional Nanosheet Heterostructures. *J Am Chem Soc* **2019**, *141* (27), 10852–10861. https://doi.org/10.1021/jacs.9b04726.

(40) Rao, S. S.; Anantharaman, T. R. Accurate Evaluation of Lattice Parameters of α-Brasses. *Curr Sci* **1963**, *32.6*, 262–263.

(41) Cordero, B.; Gómez, V.; Platero-Prats, A. E.; Revés, M.; Echeverría, J.; Cremades, E.; Barragán, F.; Alvarez, S. Covalent Radii Revisited. *Journal of the Chemical Society. Dalton Transactions* **2008**, No. 21, 2832–2838. https://doi.org/10.1039/b801115j.

TOC Graphic

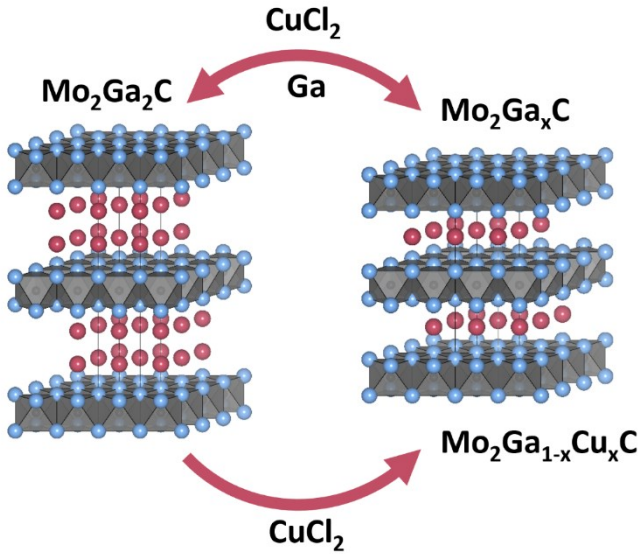

Mo_2Ga_2C is a layered carbide that is closely related to the large family of MAX phases, with the difference of exhibiting two atomic layers on the *A*-site. By using $CuCl_2$ it is possible to selectively etch one atomic layer from Mo_2Ga_2C to obtain MAX phase Mo_2GaC. Depending on the amount of Lewis acid, the Ga-content is variable and the incorporation of copper into the crystal structure can be realized. In turn, the 221 structure can be recovered by reacting Mo_2GaC with gallium.